# Applications of an Euler Aerodynamic Method to Free-Vortex Flow Simulation

P. Raj,* J. M. Keen,† and S. W. Singer†
*Lockheed Aeronautical Systems Company, Burbank, California*

**A three-dimensional Euler aerodynamic method (TEAM) is used to simulate the interaction of free vortices with lifting surfaces. The free vortices considered here arise from flow separation along sharp leading edges of slender swept wings at moderate-to-high angles of attack and shed in the wake behind lifting wings. Computed results for a 74 deg delta wing, a 75/62 deg double-delta wing body, and a canard-wing-body configuration are correlated with experimental data to evaluate TEAM's capabilities. In all cases, the flow is impulsively started and the vortices are automatically captured. Sensitivity of the computed solutions to numerical dissipation associated with TEAM's cell-centered finite-volume algorithm is investigated. Also, the effect of grid density on computations is shown. The results provide an added measure of confidence in TEAM's abilities in simulating the free-vortex flows and also point out some of its limitations.**

## Introduction

THE accurate computational simulation of flows dominated by free vortices is of great importance for aircraft design. Wakes and leading-edge separated vortices are typical examples of free vortices. Supersonic-cruise aircraft invariably exhibit leading-edge separated vortices during low-speed flight and transonic maneuvering at moderate-to-high angles of attack. Some of these aircraft may also have a close-coupled canard-wing configuration where the influence of canard wake on the wing is of critical importance. At present, a designer usually relies upon extensive and costly wind-tunnel tests for necessary data. Reliable and efficient computational methods for modeling free-vortex flows are needed to complement experimental tests.

Research on free-vortex flow simulation has produced many computational methods. At one end of the spectrum are the vortex-lattice[1-4] and free-vortex sheet (FVS) methods[5,6] based on the linearized potential-flow formulation. In these methods, the vortices have to be explicitly modeled either indirectly, using the suction analogy of Polhamus,[7] or directly, using singularities[4,5] whose final distribution and strengths are iteratively determined. At the other end of the spectrum are field methods based on the Reynolds-averaged Navier-Stokes (RANS) equations[8-10] that provide an essentially complete fluid-dynamic model. The free vortices evolve naturally as a part of the solution of these equations. However, the available methods are not well-suited for routine practical applications due to the exorbitant requirements of computational resources. An even more important consideration is the insufficient reliability of the RANS solutions of complex vortical flows due to the empiricism of the turbulence models.[11]

Recent advances in numerical algorithms to solve the inviscid nonlinear Euler equations[12,13] provide an attractive and cost-effective alternative to using the RANS methods for engineering applications. Several investigations[14-17] have demonstrated the ability of Euler methods to capture regions of rotational flow automatically. However, a number of related issues remain to be fully resolved; some of these are addressed in this paper. For instance, the numerical dissipation in Euler methods appears to be the primary source of vorticity production.[17] Of course, once the vorticity is thus introduced into the flowfield, an Euler method can, in principle, accurately model its dynamics. Consequently, sensitivity of vortical flow solutions to numerical dissipation is an area of concern. This issue is specifically addressed here for low-speed vortical flow about a delta wing and a double-delta wing body. The effect of grid density is also investigated for these two cases. In addition, solutions for a canard-wing-body configuration are presented. For all analyses, the three-dimensional Euler aerodynamic method (TEAM) code[18] is used.

## Objectives

The primary objectives of this investigation are two-fold: 1) to obtain a better understanding of TEAM's capabilities for

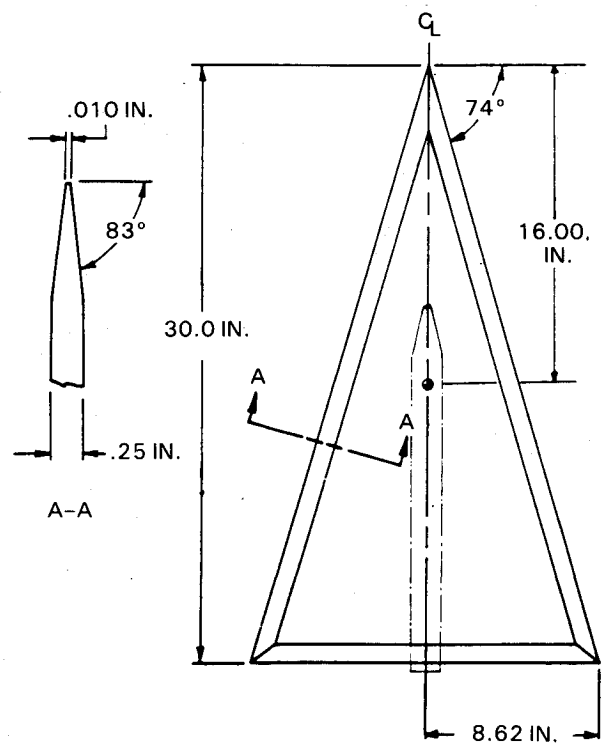


**Fig. 1 74 deg delta wing.**

Presented as Paper 88-2517 at the AIAA 6th Applied Aerodynamics Conference, Williamsburg, VA, June 6-8, 1988; received Jan. 7, 1989; revision received and accepted for publication March 9, 1990. 

*R&D Engineer, Computational Aerodynamics Group, Aerodynamics Department. Senior Member AIAA.

†Aerodynamicist, Computational Aerodynamics Group, Aerodynamics Department.

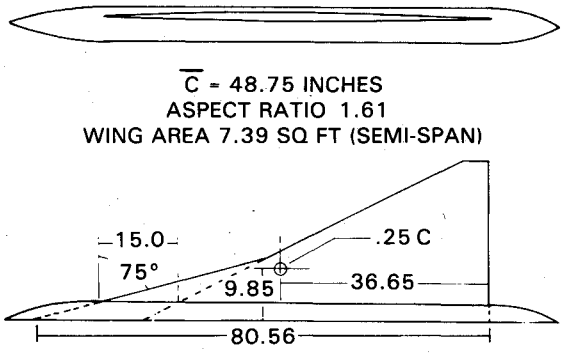


**Fig. 2 75/62 deg double-delta wing body.**

modeling free-vortex flows; and 2) to further evaluate the sensitivity of TEAM computations to numerical dissipation and grid density.

## Approach

The approach involves correlating TEAM computations with experimental data for three test cases: 1) a 74 deg delta wing (Fig. 1); 2) a 75/62 deg double-delta wing body (Fig. 2); and 3) a canard-wind-body configuration (Fig. 3) with the canard in position 1 and the wing in position 6. Both the wing and the canard have flaps deflected 5 deg about the 80% chord location.

The delta wing is analyzed at a freestream Mach number ($M_\infty$) of 0.3 and 10, 20, 30, 35, and 40-deg angle of attack $\alpha$. The wing is also analyzed in side slip at a fixed value of $\alpha$, namely, 20 deg. The double-delta wing-body configuration is analyzed at $M_\infty = 0.3$ and $\alpha$ ranging from 5 to 30 deg. For both cases, the effect of three numerical dissipation schemes on the solutions is investigated by comparing the solutions with each other and with experimental data. Also, solutions for both cases are obtained using two grids each to study the grid-density effect. The canard-wing-body configuration, canard-off and canard-on, is analyzed at $M_\infty = 0.6$ and 0.9 and $\alpha = 4$ deg. Correlations of computed and experimental data are presented to illustrate the capabilities and limitations of the code.

## Methodology

The TEAM code solves the Euler equations using the finite-volume explicit multistage time-stepping algorithm proposed by Jameson et al.[12] The finite-volume formulation essentially decouples the flow solver from grid generation. The grid may be constructed in any convenient manner; only the Cartesian coordinates are required by the solver. The TEAM code can accommodate multizone patched grids of arbitrary topologies thereby facilitating analysis of complex geometries. Across a zonal interface, three classes of grid patching are allowed: 1) one-to-one nodal point matching; 2) nodal points of one grid being an ordered subset of the other grid; and 3) mismatched nodal point distributions. The basic features of the flow-solver algorithm and the grid generation procedures used are highlighted below. Additional details can be found in Refs. 18–20.

### Flow Solver

TEAM's flow-solver algorithm requires that the region surrounding a given configuration be subdivided into small hexahedral cells. In each cell, the semidiscrete approximations to the time-dependent Euler equations, representing mass, momentum, and energy conservation, are integrated in time using a multistage scheme. Convergence to steady state is typically achieved in a few hundred time steps using local rather than global minimum step size. Enthalpy damping[12,21] and implicit residual smoothing[22] further reduce the number of steps required to reach the steady state. For spatial discretization, the flow variables are defined at cell centers and fluxes are computed at cell faces. This formulation is equivalent to a central-difference scheme, which is formally second-order accurate for smooth grids. This scheme has to be augmented by numerical dissipation terms (also known as artificial viscosity) to suppress its well-known tendency for odd-even point decoupling, to capture shocks, and to minimize pre- and post-shock oscillations. Appropriate nonreflecting boundary conditions are used at the far-field boundaries.[15,22] A no-normal-flow condition is imposed on the solid surface.

The dissipation terms can be constructed in a variety of ways. Three of them are included in TEAM: 1) standard adaptive dissipation (SAD); 2) modified adaptive dissipation (MAD); and 3) flux-limited adaptive dissipation (FAD). Their mathematical formulations are outlined in the Appendix. Both SAD and MAD schemes use blended first and third differences, as proposed by Jameson et al.[12] Differences in scaling factors lead to an overall lower level of dissipation for the MAD scheme compared to the SAD scheme. The FAD scheme employs only third differences with limiters, as suggested by Jameson.[23] It affords total variation diminishing property and nonoscillatory shock capture. All three schemes use two user-specified parameters, VIS-2 and VIS-4, to control the level of dissipation. For the SAD and MAD schemes, the VIS-4 parameter controls background dissipation needed to suppress high-frequency errors, whereas the VIS-2 parameter is used to minimize wiggles and overshoots near shocks and stagnation points. For the FAD scheme, the value of VIS-4 determines a threshold and VIS-2 is adjusted to ensure that there is enough dissipation to eliminate oscillations near shocks.

### Grid Generation

For the present investigation, the grids were generated using three methods that are part of the TEAM code. These methods and ways of using them are described in detail in Ref. 19. Their application to the three test cases used in this study is summarized below.

*Delta Wing*

An H-O-type grid was generated in two steps. First, two-dimensional O-type grids were constructed using the HYPERGRID code (based on hyperbolic differential equations) at a few selected cross sections between the apex and the trailing edge. The apex and trailing-edge grids were then duplicated at the upstream and downstream boundaries, respectively. In the second step, the TFI code (based on algebraic transfinite interpolations) was used to generate the three-dimensional field grid by interpolating a total of six

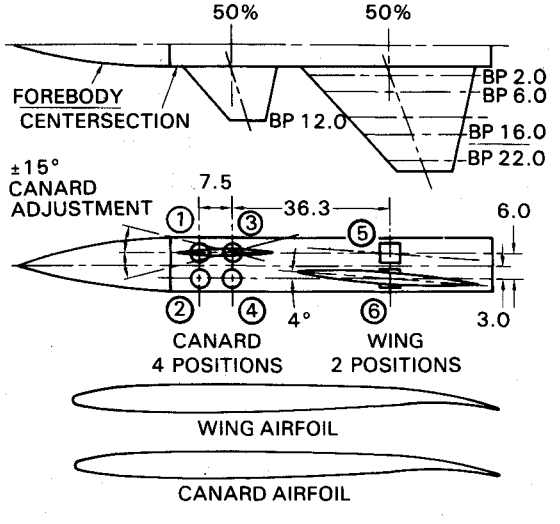


**Fig. 3 Canard-wing-body configuration.**

two-dimensional grids. The coarse grid for half the wing had 66 H-planes, each with 30 O-curves. Each O-curve was defined by 37 nodes, resulting in a total of 73,260 nodes. Note that the grid contains a singular line emanating from the apex and terminating at the upstream boundary. A second grid with 85,470 nodes was generated by increasing the number of O-curves to 35 and clustering them closer to the wing surface.

*Double-Delta Wing Body*

The PACMAPS II code (based on parabolic conformal mapping with shearing) was used to generate two C-H grids about the double-delta wing-body (DDWB) configuration. Spanwise locations of 21 H-planes spanning the wing between the wing-body junction and the tip were prescribed and held fixed for both grids. The break in the leading-edge sweep could, therefore, be preserved in the final surface grid. Both grids had 33 H-planes. For the coarse grid, each H-plane had 33 C-curves and each curve had 97 nodal points, resulting in a total of 105,633 nodes. The wing surface was defined by a 61 × 21 grid. A refined grid with 234,465 points was generated by increasing the number of C-curves to 49 and the number of nodes on each curve to 145. The wing surface was then defined by a 91 × 21 grid. The refined grid was subdivided into three zones to facilitate computation on a CRAY X-MP computer with four mega-words of core memory.

*Canard Wing Body*

The TFI code (based on a transfinite interpolation procedure) was used to generate a five-zone grid with 491,232 nodal points around the canard-wing-body configuration. All five zones were of H-H topology, with 168 H-planes between the upstream and downstream boundaries, and 34 H-planes between the plane of symmetry and the outboard side boundary. Thirteen H-planes spanned the canard surface between the canard/body junction and the tip. In every H-plane, the upper and lower surfaces were each defined by 34 nodes. The corresponding numbers for the wing were 22 H-planes and 38 nodes.

**Analysis Procedure**

For all cases, the flow was impulsively started, i.e., the flow variables, namely, density, three Cartesian components of momentum, static pressure, and total energy, in all the cells were initialized to freestream conditions. No Kutta condition was explicitly applied. A four-stage scheme with coefficients 1/4, 1/3, 1/2, and 1 was used for time integration. The implicit residual smoothing was performed at each stage using 0.75 as the smoothing parameter in all three index directions, with the Courant-Friedrichs-Lewy (CFL) number set at 6.0. The enthalpy damping parameter was 0.1. Following each time step, the average residual (the root-mean-square value of the net

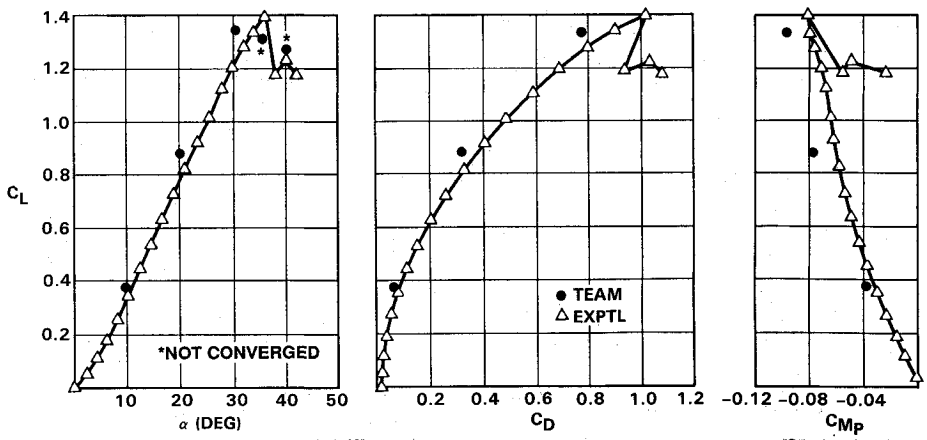


Fig. 4 Comparison of computed and measured lift, drag, and pitching moment coefficients for 74 deg delta wing; $M_\infty = 0.3$.

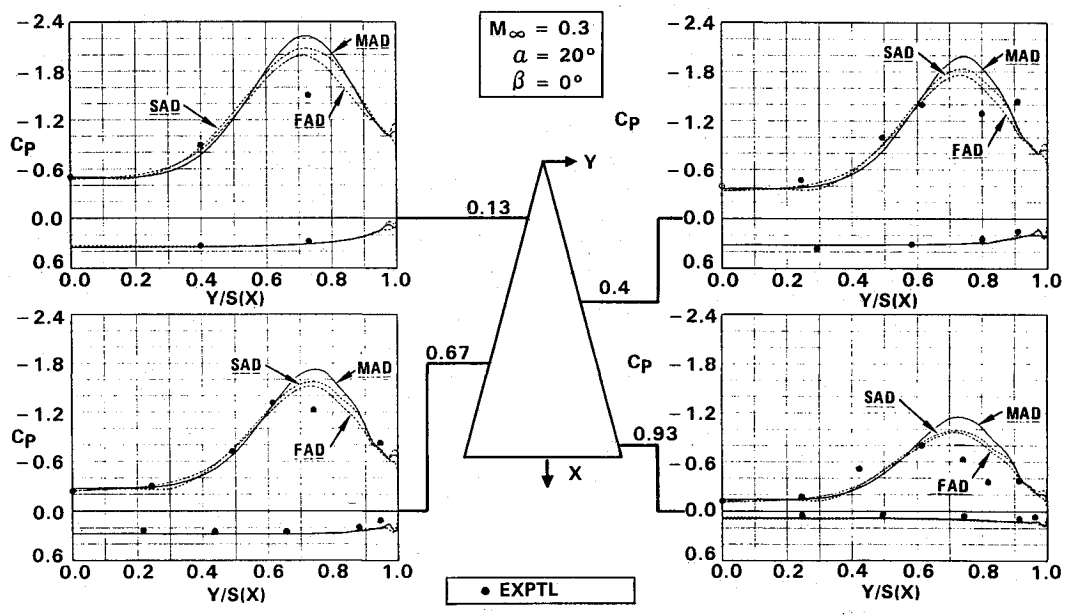


Fig. 5 Sensitivity of TEAM computations to numerical dissipation for 74 deg delta wing; $M_\infty = 0.3$, $\alpha = 20$ deg, $\beta = 0$ deg.

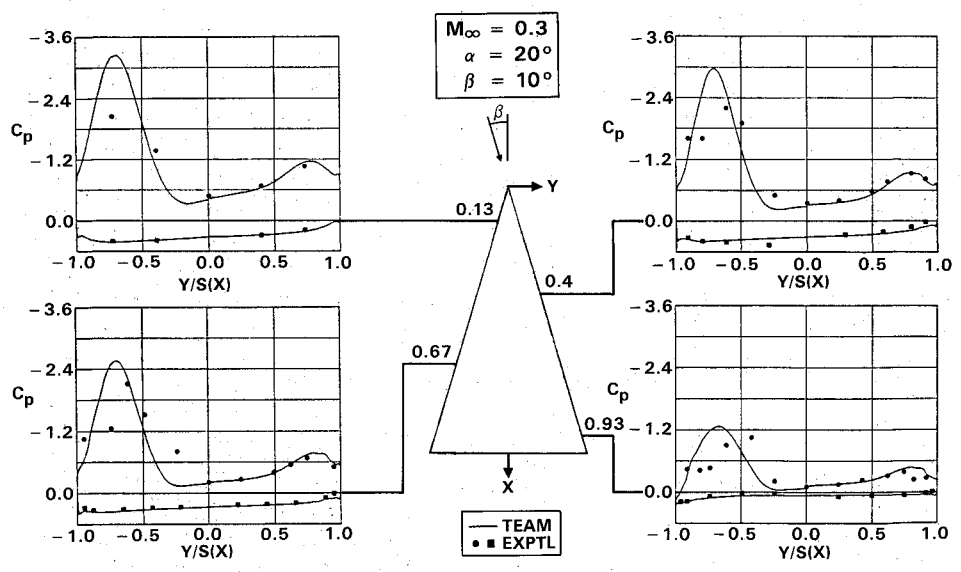


Fig. 6 Crossplane surface pressure distribution for 74 deg delta wing; $M_\infty = 0.3$, $\alpha = 20$ deg, $\beta = 10$ deg.

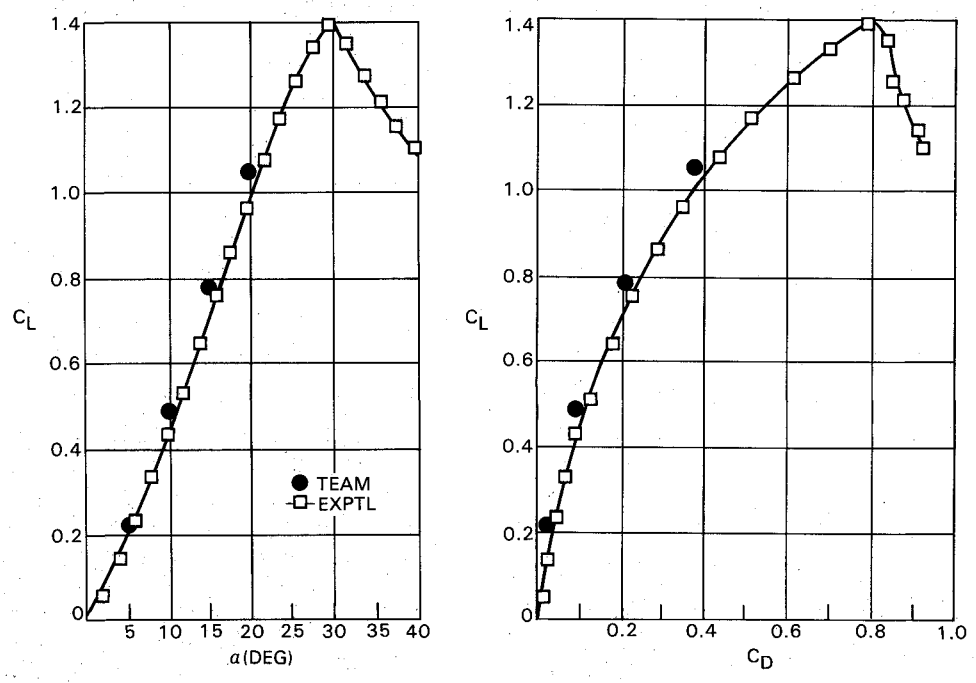


Fig. 7 Computed and measured lift and drag coefficients for 75/62 deg double-delta wing body; $M_\infty = 0.3$, $33 \times 97 \times 33$ coarse C-H grid.

mass flux) was checked to determine whether the solution reached a steady state. The time marching stopped if a prespecified convergence criterion was met or after a prescribed number of steps. The code has a provision to restart the solution process, if desired, to perform additional steps. Unless otherwise noted, the average residual was reduced by approximately four orders of magnitude for the solutions presented in the next section.

## Results and Discussion

Correlations of computed solutions and measured data for the three test cases are presented in this section. The effects of varying the numerical dissipation schemes and the grid density are discussed.

### 74 deg Delta Wing

The computed lift, drag, and pitching moment coefficients for the symmetrical-flow analysis at $M_\infty = 0.3$ and $\alpha = 10$, 20, 30, 35, and 40 deg are compared with the experimental data of Wentz[24] in Fig. 4. Only half the wing was analyzed using a 85,470-node grid. The MAD scheme was used with VIS-2 of 0.05 and VIS-4 of 2.0 for $\alpha \leq 20$ deg and 2.5 for higher $\alpha$. The computed values for $\alpha$ up to 30 deg agree well with the measured data, considering that the viscous effects are absent from the computations.

For $\alpha = 35$ and 40 deg, converged solutions were not obtained. This does not imply that the solution process diverged, only that steady-state solutions could not be obtained. The average residuals dropped approximately two to three orders of magnitude and then remained essentially unchanged. The lack of convergence could be traced to localized vortex instabilities that caused the values of the aerodynamic coefficients to fluctuate as the solution process advanced in time. Fluctuations in the pitching moment coefficient were the most noticeable. The amplitude of fluctuation was relatively larger for $\alpha = 40$ deg than for $\alpha = 35$ deg. Similar lack of convergence was observed for the double-delta wing-body case (described below), as well as in other investigations using

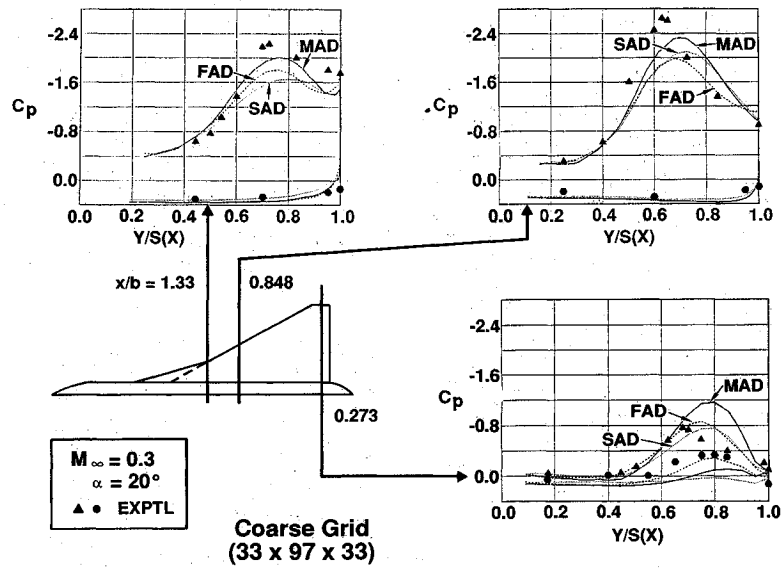


Fig. 8 Sensitivity of coarse-grid TEAM computations to numerical dissipation for 75/62 deg double-delta wing body; $M_\infty = 0.3$, $\alpha = 20$ deg.

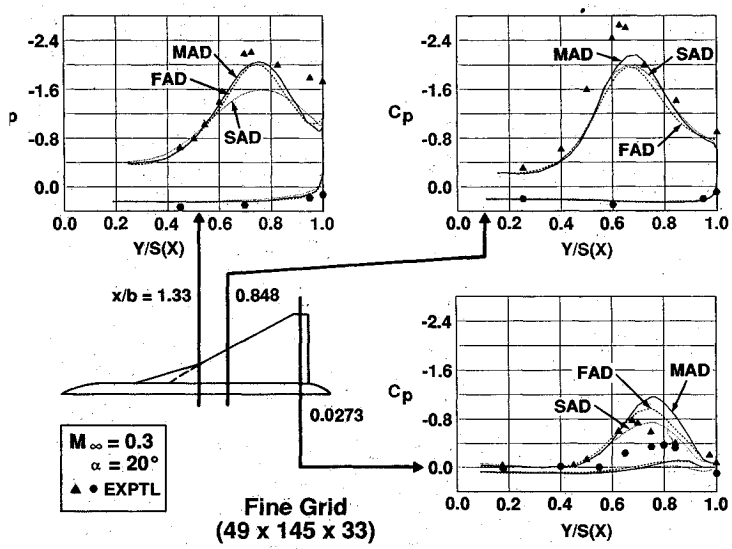


Fig. 9 Sensitivity of fine-grid TEAM computations to numerical dissipation for 75/62 deg double-delta wing body; $M_\infty = 0.3$, $\alpha = 20$ deg.

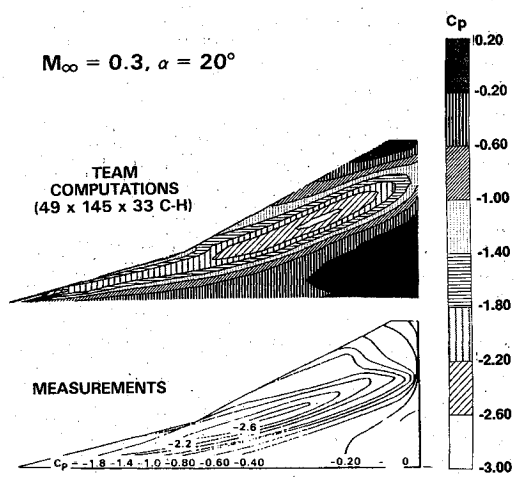


Fig. 10 Correlation of computed and measured surface pressure contours for 75/62 deg double-delta wing body; $M_\infty = 0.3$, $\alpha = 20$ deg.

TEAM.[17,25] Further investigation of this phenomenon is continuing. Note that the water-vapor patterns for $\alpha = 35$ and 40 deg (Figs. 46 and 47 in Ref. 24) strongly suggest vortex breakdown.

Typical correlations of the computed surface pressures with measured data for $\alpha = 20$ deg are shown in Fig. 5 at four crossplane stations, namely, $X/C_r = 0.133$, 0.4, 0.667, and 0.93; here, $X$ is distance from the apex and $C_r$ is the root chord. In the same illustration, computations corresponding to the three dissipation schemes, namely, SAD, MAD, and FAD, are also shown. The MAD scheme solutions show the lowest pressure levels, confirming the overall lower levels of dissipation associated with it. The same values of VIS-2 (0.05) and VIS-4 (2.0) were used for all schemes. A comparison of the solutions obtained using grids wtih 85,470 and 73,260 nodes (not shown here) indicated only marginal differences. Of course, somewhat better resolution of the flowfield was obtained using the finer grid. Note that the computed results fail to model the effect of secondary vortices whose presence is strongly suggested by the measured data.

The delta wing was also analyzed in side slip with $\alpha = 20$ deg and $M_\infty = 0.3$ using a two-zone grid, one zone

each for left and right halves. Each zone had 85,470 nodes. The crossplane pressures for a side-slip angle $\beta$ of 10 deg are correlated with experimental data in Fig. 6. Good agreement is observed on the lower surface and the downwind side of the upper surface. On the upwind side of the upper surface, the computed pressures show higher peaks than the measured ones. This is most likely due to the absence of secondary vortices (and other viscous effects) in the computations. For a higher value of $\beta$, namely, 25 deg, no converged solution was obtained. The experimental data[24] suggest vortex breakdown for side-slip angles greater than 20 deg. Further investigations are continuing.

#### 75/62 deg Double-Delta Wing Body

The DDWB configuration was analyzed at $M_\infty = 0.3$ and $\alpha = 5$, 10, 15, 20, 25, and 30 deg. Only half of the configuration was analyzed using a 105,633 node grid. The MAD scheme was used with VIS-2 set at 0.05 and VIS-4 at 2.0. Computed lift and drag coefficients for angles of attack up to 20 deg compare well with the measured values of Wentz and

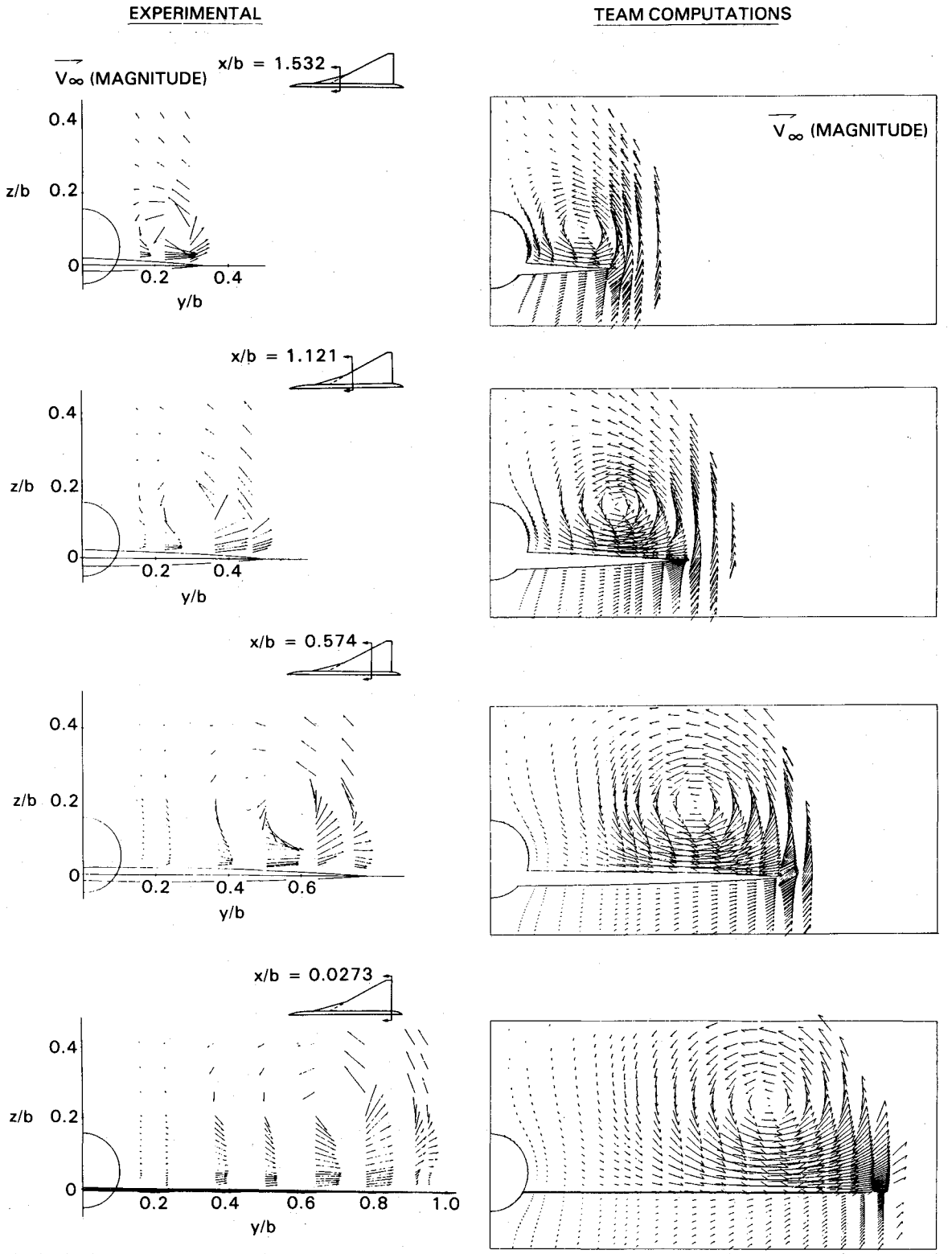


Fig. 11 Correlation of computed and measured crossplane velocity fields for 75/62 deg double-delta wing body; $M_\infty = 0.3$, $\alpha = 20$ deg.

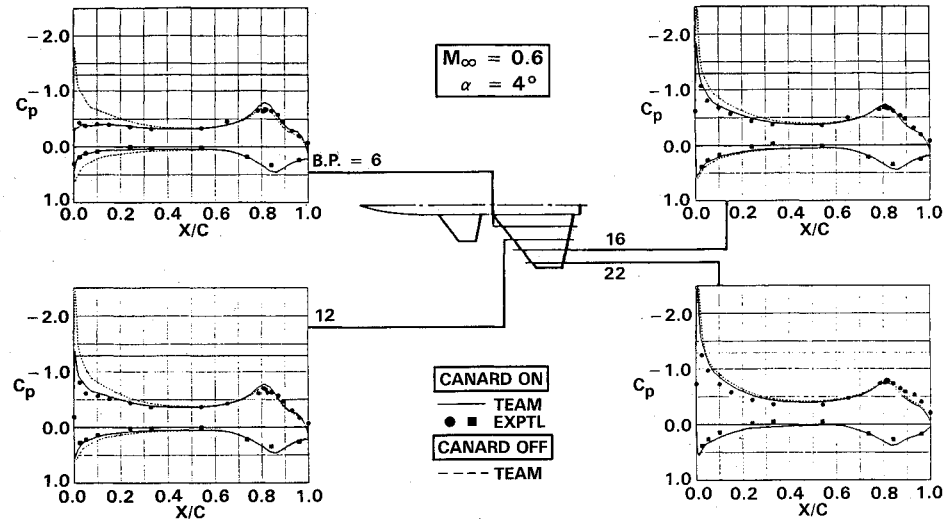


Fig. 12 Computed and measured wing surface pressures for canard-wing-body configuration; $M_\infty = 0.6$, $\alpha = 4$ deg.

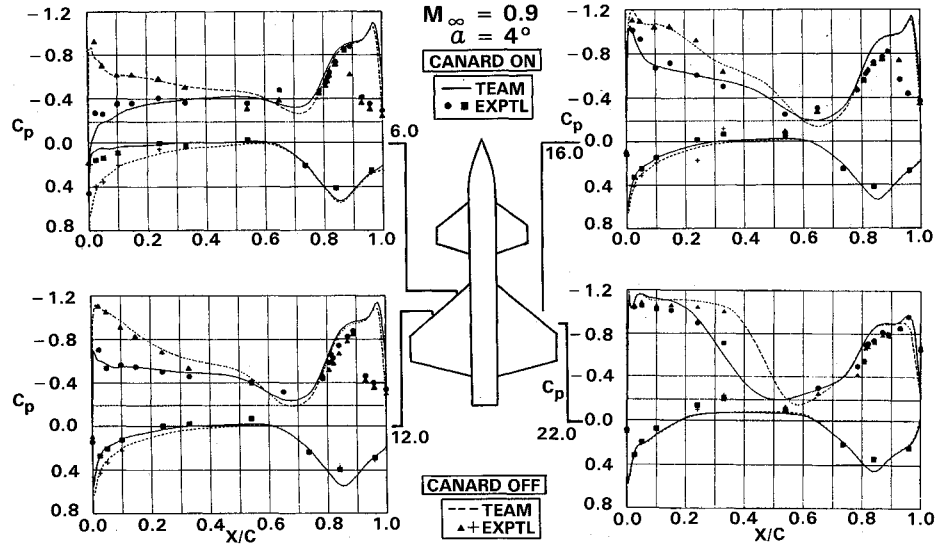


Fig. 13 Computed and measured wing surface pressures for canard-wing-body configuration; $M_\infty = 0.9$, $\alpha = 4$ deg, $168 \times 84 \times 34$ H-H grid.

McMahon,[26] as shown in Fig. 7. For $\alpha = 25$ and 30 deg, no converged solution was obtained due to localized vortex instabilities. The behavior of the solution process was similar to the one reported above for the delta wing. The amplitude of fluctuation in the values of the aerodynamic coefficients was larger for $\alpha = 30$ deg than for 25 deg.

The 20 deg angle-of-attack case was selected for a more extensive study because measured crossplane velocity fields as well as surface pressures are given in Ref. 26. The present study involved analyses using all three numerical dissipation schemes, as well as two grids with 105,633 and 234,465 nodes. The values of VIS-2 and VIS-4 were fixed at 0.05 and 2.0, respectively, for both the SAD and FAD schemes. However, when the MAD scheme was used, the values had to be raised to 0.15 and 4.0 to obtain converged solutions.

Sensitivity of the coarse-grid solutions to the numerical dissipation schemes is shown in Fig. 8, where the computed surface pressure coefficients are correlated with experimental data at three crossplane stations. Here $X$ is the distance from the wing trailing edge, and $b$ is the semispan. Similar results for the fine-grid computation are shown in Fig. 9. These results further confirm that the MAD scheme is the least dissipative one. In general, all solutions exhibited the primary vortical features of the flowfield but exhibited discrepancies from the measured data. The lack of viscous effects in the present simulation is the most likely cause for this discrepancy.

In Fig. 10, the surface pressure contours for the fine-grid solution are correlated with the measured ones. The computed velocity fields at four crossplane stations are compared with the corresponding experimental data in Fig. 11. These correlations demonstrate the ability of the TEAM code to simulate overall features of vortical flow about the double-delta wing.

### Canard Wing Body

Flow about the canard-wing-body configuration was simulated at $M_\infty = 0.6$ and 0.9 and $\alpha = 4$ deg. Only half of the configuration was analyzed, using a five-zone grid with 491,232 nodal points. The grids for both canard-on and -off configurations contained the same total number of nodes. The SAD scheme was used with VIS-2 set at 0.25 and VIS-4 at 1.5.

Correlations of computed surface pressures and measured data of Stewart[27] at four wing sections are shown in Fig. 12 for $M_\infty = 0.6$ and $\alpha = 4$ deg. The effect of canard wake in reducing the pressure peak on the inboard wing stations is quite effectively modeled by the TEAM code. Similar results for 0.9 Mach number are shown in Fig. 13. Overall agreement

between the computations and the experimental data is quite good, with the exception of the shock location. The computed shock is located approximately 10% aft of the measured one. However, this is typical of inviscid simulations of flows exhibiting significant shock/boundary-layer interaction. For the present case, effects of such an interaction are seen in the measured data but not simulated in the TEAM computations.

## Concluding Remarks

The results presented in this paper demonstrate the capabilities of TEAM to simulate free-vortex flows typified by leading-edge separated vortices associated with sharp-edged swept wings and wakes shed behind wings with sharp trailing edges. The leading-edge separated vortices are automatically captured and not explicitly modeled, as in methods based on potential-flow formulations such as the free-vortex sheet technique.

Sensitivity of the computations to three numerical dissipation schemes, namely, standard adaptive dissipation, modified adaptive dissipation, and flux-limited adaptive dissipation, was investigated. Based on the correlations of the computed results and experimental data for the 74 deg delta wing in symmetrical and asymmetrical flight and the 75/62 deg double-delta wing body, both at 0.3 Mach number, the MAD scheme was found to be the least dissipative. These results, combined with those of other related investigations, suggest that the TEAM code could be used for engineering applications to simulate leading-edge separated flows as long as 1) the wing leading edges are sharp, and 2) the secondary and tertiary vortices do not significantly interact with the primary vortex.

Use of the TEAM code for simulating free-vortex dominated flows appears to be an attractive alternative to using the RANS codes, which require greater computational resources and suffer from empiricism of turbulence modeling. This is especially true for flows that are practically Reynolds number independent. Further studies are continuing to obtain a more comprehensive understanding of the capabilities and limitations of the TEAM code.

## Appendix

### Governing Equations

For an arbitrary control volume $\Omega$ enclosed by a surface of area $A$, the unsteady integral form of the Euler equations is expressed as

$$\frac{\partial}{\partial t}\int_{\Omega} Q\,\mathrm{d}\Omega + \int_{A} F\cdot\hat{n}\,\mathrm{d}A = 0 \tag{A1}$$

where $Q=[\rho,\rho u_m,\rho E]^T$, and

$$F\cdot\hat{n} = \begin{bmatrix} (\rho u_m)\boldsymbol{n}_m \\ (\rho u_l u_m + p\delta_{lm})\boldsymbol{n}_m \\ (\rho u_m H)\boldsymbol{n}_m \end{bmatrix} \tag{A2}$$

The standard summation notation is used in writing these equations. The subscript $m$ (or $l$) = 1,2,3 corresponds to the Cartesian $X$, $Y$, $Z$ coordinates, respectively; $\rho$ denotes density; $u_m$ are Cartesian velocity components; $E$ is total energy; the unit vector normal to the surface is denoted by $\boldsymbol{n}_m$; $H=E+p/\rho$ is total enthalpy; and the static pressure $p$ is given by the equation of state as

$$p=(\gamma-1)\rho[E-(1/2)u_m u_m + H_\infty] \tag{A3}$$

where $\gamma$ is the ratio of specific heats. The quantities on the right-hand side of Eq. (A2) are evaluated at cell centers and then averaged to determine the appropriate fluxes at cell faces.

The semidiscrete form of Eq. (A1) may be written as

$$\frac{\mathrm{d}}{\mathrm{d}t}(\Omega_{I,J,K}Q_{I,J,K}) + F_{I,J,K} = 0 \tag{A4}$$

where $F$ is the net convective flux for the cell that is uniquely identified in the index space by the subscripts $I$, $J$, and $K$. The cell faces are denoted by adding or subtracting one-half from the corresponding cell index. The set of coupled ordinary differential equations, Eq. (A4), is solved by a multistage time-stepping procedure.

### Numerical Dissipation

Equation (A4) is augmented by numerical dissipation for which the following three options exist in TEAM.

*Standard Adaptive Dissipation*

This scheme is based on a blending of first and third differences in each of the three parametric index directions.[12] The $J$-direction dissipative flux at the interface between two cells identified by $(I,J,K)$ and $(I,J+1,K)$ sets of indices is written as

$$\mathrm{d}_{I,J+1/2,K} = \varepsilon_2 e_{I,J+1/2,K} - \varepsilon_4(e_{I,J+3/2,K} - 2e_{I,J+1/2,K} + e_{I,J-1/2,K}) \tag{A5}$$

where

$$e_{I,J+1/2,K} = \alpha(Q_{I,J+1,K} - Q_{I,J,K}) \tag{A6a}$$

$$\alpha = 1/2[\Lambda_{I,J,K} + \Lambda_{I,J+1,K}] \tag{A6b}$$

$$\Lambda_{I,J,K} = \lambda^I_{I,J,K} + \lambda^J_{I,J,K} + \lambda^K_{I,J,K} \tag{A6c}$$

Here, $\lambda^I$, $\lambda^J$, $\lambda^K$ are the spectral radii of the flux-Jacobian matrices in the $I$, $J$, and $K$ directions, respectively. The coefficients of the first- and third-difference terms in Eq. (A5) are constructed as follows:

$$\varepsilon_2 = \kappa_0 \bar{\nu}_{I,J+1/2,K} \tag{A7a}$$

$$\varepsilon_4 = \max(0, \kappa_1 - \varepsilon_2) \tag{A7b}$$

where

$$\bar{\nu}_{I,J+1/2,K} = \max(\nu_{I,J+2,K}, \nu_{I,J+1,K}, \nu_{I,J,K}, \nu_{I,J-1,K})$$

$$\nu_{I,J,K} = \frac{|p_{I,J+1,K} - 2p_{I,J,K} + p_{I,J-1,K}|}{|p_{I,J+1,K} + 2p_{I,J,K} + p_{I,J-1,K}|}$$

A user-specified coefficient, VIS-2, defines $\kappa_0$ and another user-input coefficient, VIS-4, divided by 64, defines $\kappa_1$. The net dissipative flux in the $J$-direction is then expressed as

$$\mathrm{D}^J_{I,J,K} = \mathrm{d}_{I,J+1/2,K} - \mathrm{d}_{I,J-1/2,K}$$

Similar expressions are written for other index directions. They are added to give the net dissipative flux for the $(I,J,K)$ cell.

*Modified Adaptive Dissipation*

This scheme is nearly identical to the standard scheme, with the exception of the scaling factor $\alpha$ in Eq. (A6b), which is redefined as

$$\alpha = (1/2)[\lambda^J_{I,J,K} + \lambda^J_{I,J+1,K}]$$

In addition, the maximum value of $\varepsilon_2$ is restricted using

$$\varepsilon_2 = \min(1/2, \kappa_0 \bar{\nu}_{I,J+1/2,K})$$

*Flux-Limited Adaptive Dissipation*

For this scheme,[23] the dissipative flux term at a cell face is expressed as

$$d_{I,J+1/2,K} = B(e_{I,J+3/2,K}, e_{I,J+1/2,K}) - 2e_{I,J+1/2,K} + B(e_{I,J+1/2,K}, e_{I,J-1/2,K}) \quad \text{(A8)}$$

where

$$\alpha = (\beta/2)(\lambda^J_{I,J,K} + \lambda^J_{I,J+1,K})$$

and the limiter operator $B$ with arguments $a$ and $b$ is defined as

$$B(a, b) = [s(a) + s(b)] \min(|a|, |b|)$$

$$s(a) = 1/2, \quad a \geq 0$$

$$= -1/2, \quad a < 0$$

If $\beta$ is set to 1/2, the scheme is excessively dissipative. This is remedied by defining $\beta$ as

$$\beta = \min(1/2, \kappa_0 + \kappa_1 \bar{v}_{I,J+1/2,K})$$

The values of $\kappa_0$ and $\kappa_1$ are specified through user-specified VIS-2 and VIS-4 parameters, respectively.

## Acknowledgments

This investigation was partly supported by the Independent Research and Development program of Lockheed Aeronautical Systems Company, Burbank, CA, and in part by U.S. Air Force Contract F33615-84-C-3005. The authors wish to thank Kent Misegades of Cray Research, Inc., Mendota Heights, MN. Without his assistance and cooperation, some of the fine-grid computations performed on the supercomputers at Mendota Heights would not have been possible.

## References

[1]Lamar, J. E., "Extension of Leading-edge-suction Analogy to Wings with Separated Flow Around the Side Edges at Subsonic Speeds," NASA TR-R-428, Oct. 1974.

[2]Lamar, J. E., and Gloss, B. B., "Subsonic Aerodynamic Characteristics of Interaction Lifting Surfaces with Separated Flow Around Sharp Edges Predicted by a Vortex-lattice Method," NASA TN-D-791, Sept. 1975.

[3]Lan, C. E., and Chang, J. F., "Calculation of Vortex Lift Effect for Cambered Wings by Suction Analogy," NASA CR-3449, July 1981.

[4]Mehrotra, S. C., and Lan, C. E., "A Theoretical Investigation of the Aerodynamics of Low-aspect-ratio Wings with Partial Leading-Edge Separation," NASA CR-145304, Jan. 1978.

[5]Johnson, F. T., Lu, P., Tinoco, E. N., and Epton, M. A., "An Improved Panel Method for the Solution of Three-dimensional Leading-edge Vortex Flows," NASA CR-3273, July 1980.

[6]Luckring, J. M., Schoonover, W. E., and Frink, N. T., "Recent Advances in Applying Free Vortex Sheet Theory for the Estimation of Vortex Flow Aerodynamics," AIAA Paper 82-0095, Jan. 1982.

[7]Polhamus, E. C., "A Concept of the Vortex Lift of Sharp Edge Delta Wings Based on a Leading-edge-suction Analogy," NASA TN-D-3767, Dec. 1966.

[8]Fujii, K., and Kutler, P., "Numerical Simulation of the Leading-edge Separation Vortex for a Wing and Strake-wing Configuration," AIAA Paper 83-1908, July 1983.

[9]Thomas, J. L., Taylor, S. L., and Anderson, W. K., "Navier-Stokes Computations of Vortical Flows Over Low-Aspect Ratio Wings," AIAA Paper 87-0207, Jan. 1987.

[10]Fujii, K., and Schiff, L. B., "Numerical Simulation of Vortical Flows over a Strake-delta Wing," AIAA Paper 87-1229, June 1987.

[11]Lakshminarayana, B., "Turbulence Modeling for Complex Shear Flows," *AIAA Journal*, Vol. 24, Dec. 1986, pp. 1900–1917.

[12]Jameson, A., Schmidt, W., and Turkel, E., "Numerical Solutions of the Euler Equations by Finite-Volume Methods Using Runge-Kutta Time-Stepping Schemes," AIAA Paper 81-1259, June 1981.

[13]Rizzi, A., "Damped Euler Equation Method to Compute Transonic Flow Around Wing-body Combinations," *AIAA Journal*, Vol. 20, Oct. 1982, pp. 1321–1328.

[14]Hitzel, S. M., and Schmidt, W., "Slender Wings with Leading-edge Vortex Separation: A Challenge for Panel Methods and Euler Solvers," *Journal of Aircraft*, Vol. 21, Oct. 1984, pp. 751–759.

[15]Raj, P., and Sikora, J. S., "Free-vortex Flows: Recent Encounters with an Euler Code," AIAA Paper 84-0135, Jan. 1984.

[16]Rizzi, A., "Computer Simulation of Non-potential Flows Around Wings," *Aeronautical Journal*, June/July 1984, pp. 238–248.

[17]Raj, P., Sikora, J. S., and Keen, J. M., "Free-vortex Flow Simulation Using a Three-dimensional Euler Aerodynamic Method," *Journal of Aircraft*, Vol. 25, Feb. 1988, pp. 128–134.

[18]Raj, P., Brennan, J. E., Keen, J. M., Mani, K. K., Olling, C. R., Sikora, J. S., and Singer, S. W., "Three-dimensional Euler Aerodynamic Method (TEAM), Volume I: Computational Method," Air Force Wright Aeronautical Laboratories, Wright-Patterson Air Force Base, OH, AFWAL-TR-87-3074, Dec. 1987.

[19]Raj, P., Brennan, J. E., Keen, J. M., Long, L. N., Sikora, J. S., and Singer, S. W., "Three-dimensional Euler Aerodynamic Method (TEAM), Volume II: Grid Generation User's Manual," Air Force Wright Aeronautical Laboratories, Wright-Patterson Air Force Base, OH, AFWAL-TR-87-3074, Dec. 1987.

[20]Raj, P., Sikora, J. S., and Olling, C. R., "Three-dimensional Euler Aerodynamic Method (TEAM), Volume III: Flow Analysis User's Manual," Air Force Wright Aeronautical Laboratories, Wright-Patterson Air Force Base, OH, AFWAL-TR-87-3074, Dec. 1987.

[21]Moitra, A., Turkel, E., and Kumar, A., "Application of a Runge-Kutta Scheme for High-speed Inviscid Internal Flows," AIAA Paper 86-0104, Jan. 1986.

[22]Jameson, A., and Baker, T. J., "Solution of the Euler Equations for Complex Configurations," AIAA Paper 83-1929, July 1983.

[23]Jameson, A., "A Nonoscillatory Shock Capturing Scheme Using Flux Limited Dissipation," Mechanical and Aerospace Engineering Report 1653, Princeton Univ., Princeton, NJ, 1983.

[24]Wentz, W. H., Jr., "Effects of Leading-edge Camber on Low-speed Characteristics of Slender Delta Wings," NASA CR-2002, Oct. 1972.

[25]Raj, P., and Long, L. N., "An Euler Aerodynamic Method for Leading-edge Vortex Flow Simulation," *Vortex Flow Aerodynamics*, NASA CP-2416, Oct. 1985, pp. 263–281.

[26]Wentz, W. H., Jr., and McMahon, M. C., "An Experimental Investigation of the Flowfields about Delta and Double-delta Wings at Low Speeds," NASA CR-521, Aug. 1966.

[27]Stewart, V. R., "Evaluation of a Propulsive Wing/Canard Concept at Subsonic and Supersonic Speeds," Rockwell International, Columbus, OH, Rept. NR82H-85, Vol. I, Aug. 1983.